16th World Conference on Earthquake Engineering, 16WCEE 2017
Santiago Chile, January 9th to 13th 2017
Paper N° 1170 (Abstract ID)
Registration Code: S-C1463189466

ASSESSMENT OF THREE VISCOUS DAMPING METHODS FOR NONLINEAR HISTORY ANALYSIS: RAYLEIGH WITH INITIAL STIFFNESS, RAYLEIGH WITH TANGENT STIFFNESS, AND MODAL

Y. Lu[(1)], G. R. Morris[(2)]

[(1)] *Software Engineer, Computers & Structures, Inc., yuan@csiamerica.com*
[(2)] *Software Development Manager, Computers & Structures, Inc., bob@csiamerica.com*
…

Abstract

This paper discusses three methods for applying linear viscous damping at the global level in nonlinear time history analysis: (1) Rayleigh damping proportional to the mass and initial stiffness matrices, (2) Rayleigh damping proportional to the mass and tangent stiffness matrices, and (3) modal damping through the dynamic nonlinear modal analysis method, also known as fast nonlinear analysis (FNA). The effect of global stiffness changes on structures modeled with the three methods is studied and compared. This paper showcases one of the limitations of Method 1 (Rayleigh damping with initial stiffness): sensitivity to the modeling of localized nonlinearity, such as frame elements that are sub-divided around the nonlinear hinges. As the sub-division around the nonlinear hinges become smaller, the damping forces in the nonlinear elements become larger and can have a significant effect on the computed forces in neighboring elements as well as global behavior. In contrast, the latter two methods are insensitive to the modeling of localized nonlinearity. Finally, the results of nonlinear response history analyses using each method is compared for a 30-story building model used for performance-based design. All structural modeling and analysis is done using the commercial software ETABS 2015. Method 3 (modal damping with FNA) gives similar results to Method 2 (Rayleigh damping with tangent stiffness) for the 30-story building model. The effect of the three methods upon the efficiency of analysis is also compared.

Keywords: Nonlinear Dynamic Analysis, Modal Damping, Rayleigh Damping, Fast Nonlinear Analysis.

1. Introduction and Motivation

In this paper, three types of global linear viscous damping models used for nonlinear time history analyses (NLTHA) are considered:

1. Mass and initial stiffness proportional Rayleigh damping, which will be referred to as RI damping. The damping matrix is a linear combination of the mass and initial stiffness matrices M and K_0, respectively.

$$C = \alpha\, M + \beta\, K_0 \tag{1}$$

The damping ratio for the nth mode, ζ_n, is

$$\zeta_n = \frac{\alpha}{2\omega_n} + \frac{\beta}{2}\omega_n \tag{2}$$

where ω_n is the circular frequency of the mode and α and β are the mass and stiffness proportional coefficients, respectively. While RI damping is classical for a linear elastic structure, the damping matrix may be non-classical for NLTHA, where the tangent stiffness may vary over time due to nonlinear behavior in the structural model.

2. Mass and tangent stiffness proportional Rayleigh damping, which will be referred to as RT damping. The damping matrix is a linear combination of the mass and tangent stiffness matrices M and K_T, respectively. It has been shown that RT damping agrees better with experimental observations than RI damping [14].

$$C = \alpha\, M + \beta\, K_T \tag{3}$$

The mass and stiffness proportional coefficients α and β are defined as for RI damping; in this paper, the coefficients α and β are computed based on the initial stiffness and are constant throughout the analysis. This damping model differs from RI damping only for NLTHA; in contrast to RI damping, RT damping maintains a classical damping matrix for nonlinear structures. Studies [2,12] have considered the case where coefficients α and β are recomputed every time step based on the tangent stiffness. However, this requires a modal analysis at every time step, an expensive operation when used for realistic structural models.

3. Modal damping. In this method, the damping is equivalent to that used in linear modal time-history analysis. A major advantage of this method is that the modal damping ratio, ζ_n, can be specified for each mode independently. In the modal space, the modal damping matrix is diagonal. The resulting damping matrix for direct-integration time history analysis is [3,16]:

$$C = M^T \left(\sum_{n=1}^{N} \frac{2\,\zeta_n\,\omega_n}{M_n} \phi_n \phi_n^T \right) M \tag{4}$$

where $\Phi = [\phi_1, \phi_2, \ldots, \phi_N]$ is a set of N mode shapes computed for the structure; and M_n, ζ_n, and ω_n are the modal mass, damping ratio, and circular frequency for mode n, respectively. Note that N may be less than the total number of modes for the structure. When used for in direct-integration time history analysis, the modal damping matrix is fully populated as opposed to the sparse form of the RI and RT damping matrix. Some implementations of modal damping approximate the damping matrix by using only the terms that fall in the bandwidth of the stiffness matrix [13]; differences between using the full and approximate modal damping matrix for direct-integration NLTHA are studied in [3]. When NLTHA is performed in the modal space, the modal damping matrix is diagonal; modal NLTHA is described in the following section.

RI damping is the most commonly used global linear viscous damping model and is available in many existing structural analysis software: e.g. [6,11,13]. Existing structural analysis software has also implemented the RT damping [6,11] and modal damping [6,11,13] methods. RI damping has limitations which have been widely studied [1-3,5,7-10,12,14,17]; an overview of the literature can be found in Jehel et al. [10]. This paper will discuss two major issues present for RI damping with a focus of studying the behavior of modal damping for these issues:

1. Linear damping forces proportional to the initial stiffness of the model may be excessive in comparison to the nonlinear resisting force, especially for yielding, cracking, or gap/hook elements. To reduce the effect of this issue, the stiffness used to construct the RI damping matrix can be reduced or neglected for nonlinear elements [13, 17] or the overall damping force can be limited [7]. Studies [8,12] have shown that RT damping successfully

limits excessive damping during post-yield behavior; however, use of RT damping can cause numerical convergence difficulties when sudden changes in stiffness occur [7].

2. Spurious damping forces can occur at degrees of freedom with no or small mass when the stiffness matrix used for stiffness-proportional damping differs from the stiffness matrix of the structure [1,3]. McKenna and Chopra [3] showed that RT and modal damping do not exhibit spurious damping at degrees of freedom with zero mass. Studies [8,16] have also shown that RI damping can provide an unrealistically high level of damping, causing artificial collapse resistance for structures at or near collapse. This paper illustrates that, because of this issue, the damping force computed with RI damping has a strong dependence on initial stiffness and discretization of nonlinear components, a behavior that RT and modal damping do not exhibit.

This paper discusses, quantitatively, the effect of global and local changes of stiffness on the damping ratio for the three damping models considered. A case study of a 30-story building model subjected to two bi-axial ground motions is presented to qualitatively assess and compare the three damping methods for use in a realistic structural model. All structural modeling and analysis is done using the commercial software ETABS 2015 (v15.2.2) using direct-integration time history analysis with RI and RT damping and nonlinear modal time history analysis with modal damping.

2. Nonlinear Modal Time History Analysis: Fast Nonlinear Analysis

In this paper, nonlinear modal time history analysis is performed using the Fast Nonlinear Analysis (FNA) method developed and described in Ibrahimbegovic and Wilson [9] and Wilson [15]. Two important features of the FNA method are: nonlinear behavior occurs only in pre-defined elements, and the time history analysis is performed using modal superposition. A short summary is presented in this section.

When using FNA, nonlinearity is restricted to predefined elements and degrees of freedom. While it is extremely efficient for structural systems which have a limited number of nonlinearities, there is no limit on the number of nonlinear elements that can be considered. For a linear elastic structure with predefined nonlinear elements, the dynamic equilibrium equations at time *t* can be written as:

$$M\,\ddot{u}(t) + C\,\dot{u}(t) + K_L\,u(t) + R_{NL}(t) = R(t) \tag{5}$$

where *M* and *C* are the mass and proportional damping matrices, respectively; and K_L is the assembled stiffness matrix of the linear elastic elements; R_{NL} is the global resisting force vector for nonlinear elements; $u(t)$, $\dot{u}(t)$, $\ddot{u}(t)$ are the relative displacements, velocities, and accelerations at time *t* with respect to the ground; and *R* is the vector of applied loads. Moving $R_{NL}$to the right-hand side:

$$M\,\ddot{u}(t) + C\,\dot{u}(t) + K_L\,u(t) = R(t) - R_{NL}(t) \tag{6}$$

A linear effective stiffness matrix, K_N, for the nonlinear elements is added to both sides of the equation. This effective stiffness is arbitrary and can be between zero and the maximum nonlinear stiffness. The resulting dynamic equilibrium equation resembles the linear elastic modal equations and all nonlinear effects are incorporated in the right-hand side:

$$M\,\ddot{u}(t) + C\,\dot{u}(t) + K\,u(t) = \hat{R}(t) \tag{7}$$

with stiffness matrix *K* and effective applied load vector, $\hat{R}(t)$:

$$K = K_L + K_N \tag{8}$$

$$\hat{R}(t) = R(t) - R_{NL}(t) + K_N\,u(t) \tag{9}$$

Modal analysis is performed using the stiffness matrix *K* and mass matrix *M*. In this paper, the load dependent Ritz-vector method is used to generate a set of *N* orthogonal modes, Φ, as suggested in [4,15]. The equilibrium equations can be written in modal form as:

$$I\,\ddot{Y}(t) + \Lambda\,\dot{Y}(t) + \Omega^2\,Y(t) = F(t) \tag{10}$$

$$F(t) = \Phi^T \hat{R}(t) = \Phi^T R(t) - \Phi^T R_{NL}(t) + \Phi^T K_N u(t) \quad (11)$$

where *Y* is the vector of modal coordinates, *I* is the identity matrix, Λ is the modal damping matrix, and Ω is the diagonal matrix of modal frequencies. Unlike linear modal time history analysis, the modal equations in Eq. (10) will be coupled through the resisting force vector for nonlinear elements, which is a function of all modal displacements. Because of this, iteration is necessary to obtain the solution of the modal equations. The decomposition to modal equations allows the damping ratio to be specified per mode.

Compared to direct integration time history analysis with a damping matrix formed by the modal properties, FNA has a few advantages:

1. Because the equations of motion are solved in the modal form, modal damping does not require formation or storage of a fully populated damping matrix or approximation of the modal damping matrix.

2. Exact, closed-form integration can be used to solve the modal equations at every iteration, removing time-step dependence due to the time stepping algorithms used. Thus, the method is not sensitive to time step to the extent that the nonlinearity is piece-wise linear over the time step.

3. The FNA method can be used without the complete set of all possible structural modes. For this reason, it is suggested to use the load dependent Ritz-vector method to determine a sufficient number of structural modes to represent the behavior of the structural response. The number of equations solved when using the FNA method may be significantly smaller than the total number of degrees of freedom in the structure, especially for structures with limited nonlinear degrees of freedom. This can result in significantly faster analysis completion time with comparable accuracy compared to direct-integration time history analysis.

However, it is important to note that the solution obtained by FNA is dependent on being able to adequately represent the behavior of the structure and nonlinear forces by the computed mode shapes. With sufficient modal representation, the results of FNA are of comparable or greater accuracy than that of direct integration [15].

3. Effect of Changes in Stiffness on Damping Ratio

In this section, the damping ratio for inelastic yielded modes is discussed for the three damping methods. For any damping matrix C, the damping ratio of the n^{th} mode is found using the modal strain energy (MSE) method [2]:

$$\zeta_n = \frac{\phi_n^T C \phi_n}{2 \omega_n \phi_n^T M \phi_n} \quad (12)$$

The damping ratios found by the MSE method are exact for a classically damped system. For a non-classically damped system, the damping ratio calculated from Eq. 12 is approximate with good accuracy for low damping ratios.

3.1 Effect of Global Changes in Stiffness

This example illustrates the effect of global stiffness change due to inelastic structural behavior using the five degree of freedom structural model studied by Charney [2]. This simplified model represents a five story structure with one degree of freedom for each story. The mass and stiffness of each floor is identical and equal to 228 kN-sec^2/m and 8.70x10^4 kN/m, respectively; Table 1 lists the natural frequencies of the structural model. For RI and RT damping, the damping coefficients α = 0.183 and β = 0.00128 so the first and third elastic modes have a damping ratio of 2%. For modal damping, all modes have a damping ratio of 2%.

To illustrate the effect of nonlinear behavior, two scenarios for damage in the structure are studied:

Case 1, Uniform Damage: The entire stiffness matrix is assumed to reduce to 50% of its original value.

Case 2, Varied Damage: The stiffness properties change non-uniformly along the height: 0.9, 0.7, 0.5, 0.3, and 0.1 times the initial stiffness of each story, top down, respectively.

The second and third columns of Table 1 lists the natural frequencies for Case 1 and 2, respectively. Figures 1(a) and (b) show the damping ratio versus circular frequency for the damaged modes for Case 1: Uniform Damage

and Case 2: Varied Damage, respectively. In the two figures, the elastic damping curves for Rayleigh and modal damping are shown in grey and the vertical dashed lines represent the original undamaged frequencies.

Table 1 – Modal Frequencies (radian/sec) of five degree of freedom structural model

Mode	Elastic: No Damage	Case 1: Uniform Damage	Case 2: Varying Damage
1	5.56	3.95	2.29
2	16.23	11.48	9.81
3	25.58	18.09	16.41
4	32.87	23.24	23.18
5	37.47	26.51	31.00

For Case 1: Uniform Damage, the damaged modal frequencies are exactly 0.7072 times the undamaged modal frequencies for all modes due to the uniform reduction in the stiffness matrix. For the two damping methods which depend only on the initial state of the structure – RI and modal damping – the damping ratio at the frequency of each damaged mode is exactly 1.414 times the original damping ratio at the original frequency of the undamaged mode. The RT damping matrix is proportional to the damaged stiffness and the damping ratios of the damaged system lies on the Rayleigh damping curve defined for the undamaged system. The damping ratios at the damaged frequencies differ from that of the corresponding initial frequencies because the frequencies have shifted toward lower values.

For Case 2: Varying Damage, RI and modal damping, which depend only on the initial state of the structure, may be non-classical when the stiffness changes. For both RI and modal damping, the damping ratios at the damaged modes are considerably larger – up to 2.5 times – than that of the corresponding undamaged modes. For this case, modal damping results in a smaller increase of damping ratio for the higher modes. As for Case 1, the damping ratio of the damaged system for the RT damping method lies on the Rayleigh damping curve defined for the undamaged system. Note that, due to the shape of the Rayleigh damping curve, the damping ratio of the first damaged mode for RT damping is twice that of the corresponding undamaged modes. For this reason, studies have suggested that Rayleigh damping constants be defined taking into account the damaged modal frequencies [2,12].

For the two cases of global stiffness change considered in this section, modal damping does not result in significant improvement over RI damping.

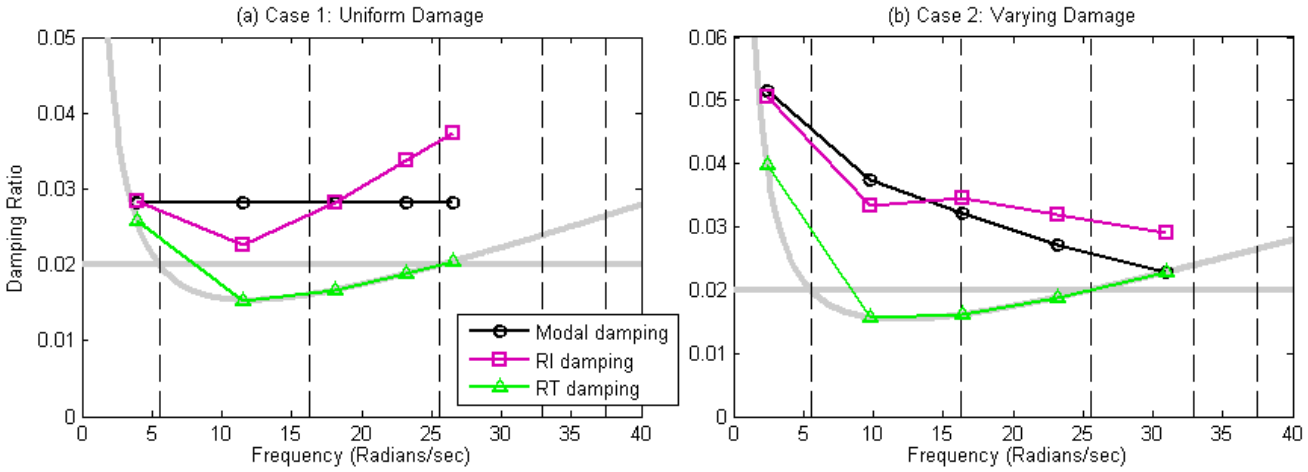

Fig. 1 – Damping ratio versus frequency for (a) Case 1: Uniform Damage and (b) Case 2: Varying Damage. The elastic damping curves for Rayleigh and modal damping are shown in grey. Vertical dotted lines show the elastic modal frequencies.

3.2 Effect of Local Inelasticity and Sensitivity to Discretization

This example considers a simple model consisting of two elements (elements A and B) in series, shown in Figure 2. Nonlinear behavior in element A is modeled using a concentrated plasticity element. Element A consists of two components: a short nonlinear component, representing the concentrated plasticity, and an elastic component. For this study, the node between the two components in beam A has a negligible non-zero mass. The model has modal frequencies of 62.81 and 1.64 rad/sec (a period of 0.1 and 0.038 sec, respectively) initially and modal frequencies of 16.38 and 1.45 rad/sec (a period of 0.38 and 0.043 sec, respectively) after yielding in the nonlinear element. For RI and RT damping, the damping coefficients α = 1.8186 and β = 1.76 x10^{-4} so the first and second elastic modes have a damping ratio of 2%. This was modeled in ETABS by using frame elements discretized (using the hinge overwrite option) around the nonlinear hinge.

Fig. 2 – Schematic of nonlinear two element model

Figure 3 shows the damping ratio for the first yielded mode using the MSE for varying values of r_h, the ratio of nonlinear component length to the total length of element A. The damping ratios for modal and RT damping are larger than 2% as discussed in section 2.1 of this paper and are not dependent on r_h. The damping ratios for RI damping increases as r_h decreases, corresponding to a decreasing size of the nonlinear component. This issue occurs because RI damping is proportional to the large initial stiffness of the nonlinear component; after the nonlinear element yields, this initial stiffness proportional part of the damping results in disproportionally large damping forces in the yielded nonlinear component. In contrast, the modal damping matrix is not significantly affected by the large initial stiffness of the nonlinear component of element A.

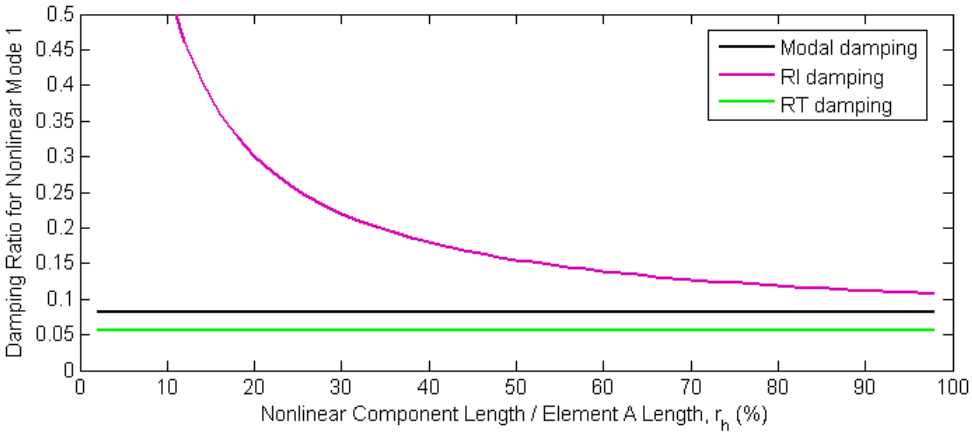

Fig. 3 – Damping ratio of the fundamental mode of the yielded system (ω = 62.8 rad/s) versus the discretization size of the inelastic portion.

Figure 4 shows applied force versus displacement at node 2 where 1.8 times the yield force was applied to node 2 over 0.9 seconds in ETABS. The yield force was 10 kips. Models with modal and RT damping showed no sensitivity to the discretization of the nonlinear hinge. The force-displacement behavior for models with RI damping showed artificial post-yield stiffness which increased with decreasing r_h. Figure 5 compares the resisting force from the nonlinear and elastic components of element A and illustrates the discrepancy between the resisting forces for models with RI damping. Equilibrium is maintained between the nonlinear and elastic components because of the large damping force in the nonlinear component, due to the accumulation of deformation in the

nonlinear component after yield and the initial stiffness-proportional damping. The 25% of the total force resisted in the nonlinear component was contributed by the damping force when 1.8 times the yield force was applied to the r_h = 1% model.

For RI damping, the sensitivity to discretization has been alleviated in existing structural analysis software [6,13] through the use of substructuring for frame (beam or column) elements with concentrated plastic hinges. For substructuring, the joint connecting the nonlinear and elastic components in element A is internal to the element and static condensation is used to get the properties of element A as a superelement. Thus, global damping would be applied for element A as a whole. This effect is also observed for distributed plasticity elements, as studied in McKenna and Chopra [3] where the damping model is shown to have significantly less influence on the response when distributed plasticity elements are used to model nonlinear structural elements.

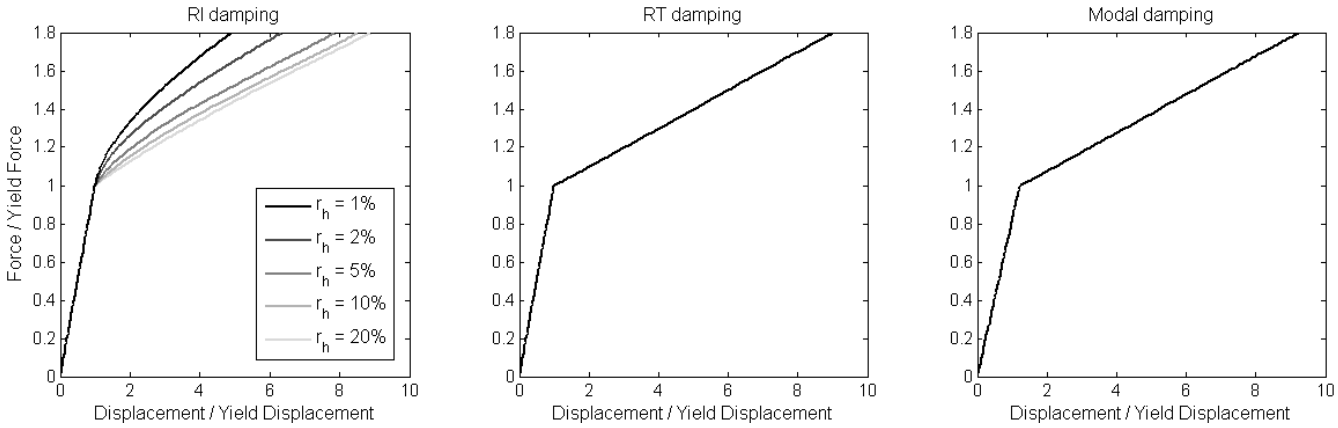

Fig. 4 – Force versus displacement response normalized by the yield force and displacement for varying r_h, ratio of nonlinear component length to total length of element A.

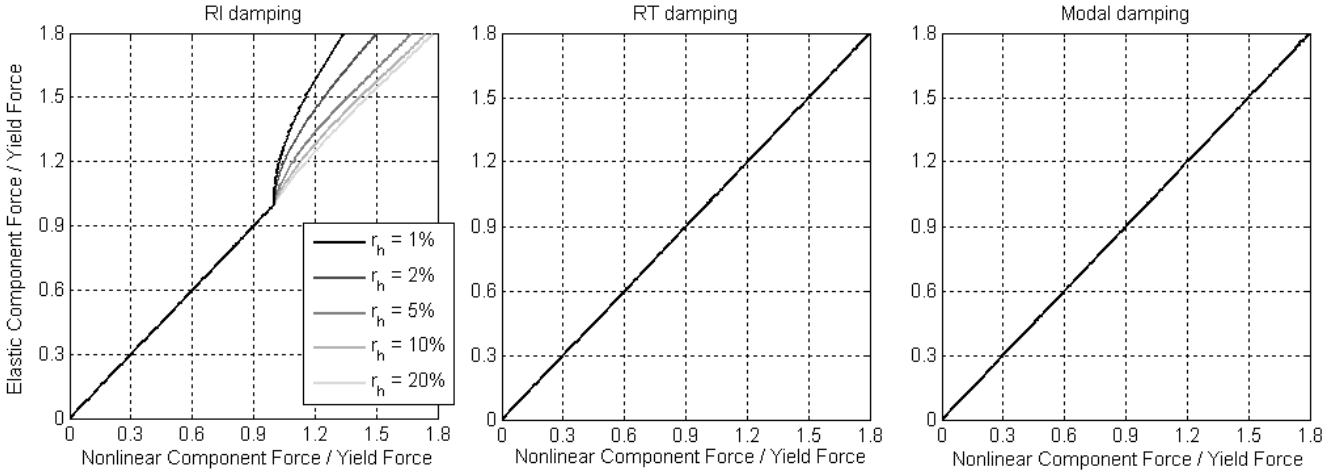

Fig. 5 – Resisting force of the elastic component vs. that of the nonlinear component, both normalized by the nonlinear yield force, for varying r_h (the ratio of nonlinear component length to total length of element A).

4. Case Study: 30-story Shear Wall Building

The 30-story building model shown in Figure 6(a) is used to qualitatively assess and compare the damping methods for use in realistic structural models. The building consists of two C-shaped reinforced concrete core walls joined by slender coupling beams at the story levels. The core walls are modeled using shell elements, and nonlinear fiber wall hinges are used in the bottom 10 stories of the model. All coupling beams over the height of the building are modeled using frame elements with nonlinear moment hinges at both ends. The slabs at each story are modeled

using linear thin shell elements and the rigid diaphragm constraint is applied at each floor level. Exterior columns are assumed to be linear elastic and are modeled with pinned supports at the ground level. The total number of unconstrained degrees of freedom in this model is 13,914; the total number of nonlinear degrees of freedom is 240. Two hinge discretization sizes are considered for the coupling beam elements: 5% and 25% of the beam length for each hinge. Wall hinges are modeled to account for the flexibilty of the entire wall element. Geometric nonlinearity was not considered. The first three modal periods are 2.386, 0.454, and 0.198 sec and 2.322, 0.514, and 0.229 seconds in the X- and Y- directions, respectively.

The 30-story building model is subjected to two ground motion excitations: LACC-NOR is the recorded far-field ground motion from the LA – Century City CC North station during the 1994 Northridge, CA earthquake with an amplitude scaling factor of 7.6 to represent a MCE-level earthquake, and SCAL-LONG is a synthetic ground motion record generated by ETABS to match the response spectrum from the recorded ground motion at the Kanti Path, Kathmandu station during the April 2015 Nepal earthquake. The SCAL-LONG excitation was selected to excite the long period modes of the structure. The acceleration response spectrum for the two ground motion excitations are shown in Figure 6(c) and (d) for the X- and Y-direction components, respectively; in this figure, LACC-NOR is shown unscaled.

RI and RT damping models are analyzed using nonlinear direct-integration time history analysis with damping parameters $\alpha = 0.0961$ and $\beta = 1.33 \times 10^{-3}$ so the first and third translational modes have a damping ratio of 2%; the Hilbur-Hughes-Taylor time stepping algorithm [4] is used with a factor of alpha = -0.05. The modal damping is analyzed using FNA with 620 modes generated using acceleration in the X- and Y- directions, gravity loading, and link forces as starting vectors for Ritz modal vector generation. 2% damping is applied in all modes with period of 0.001 sec or more and 20% damping is applied in modes with period of less than 0.001 sec; this is specified to reduce high frequency behavior in the model and has negligible effect on response behaviors with frequency less than 100 Hz. Analysis for both ground motion excitations was computed with a maximum time step of 0.02 sec.

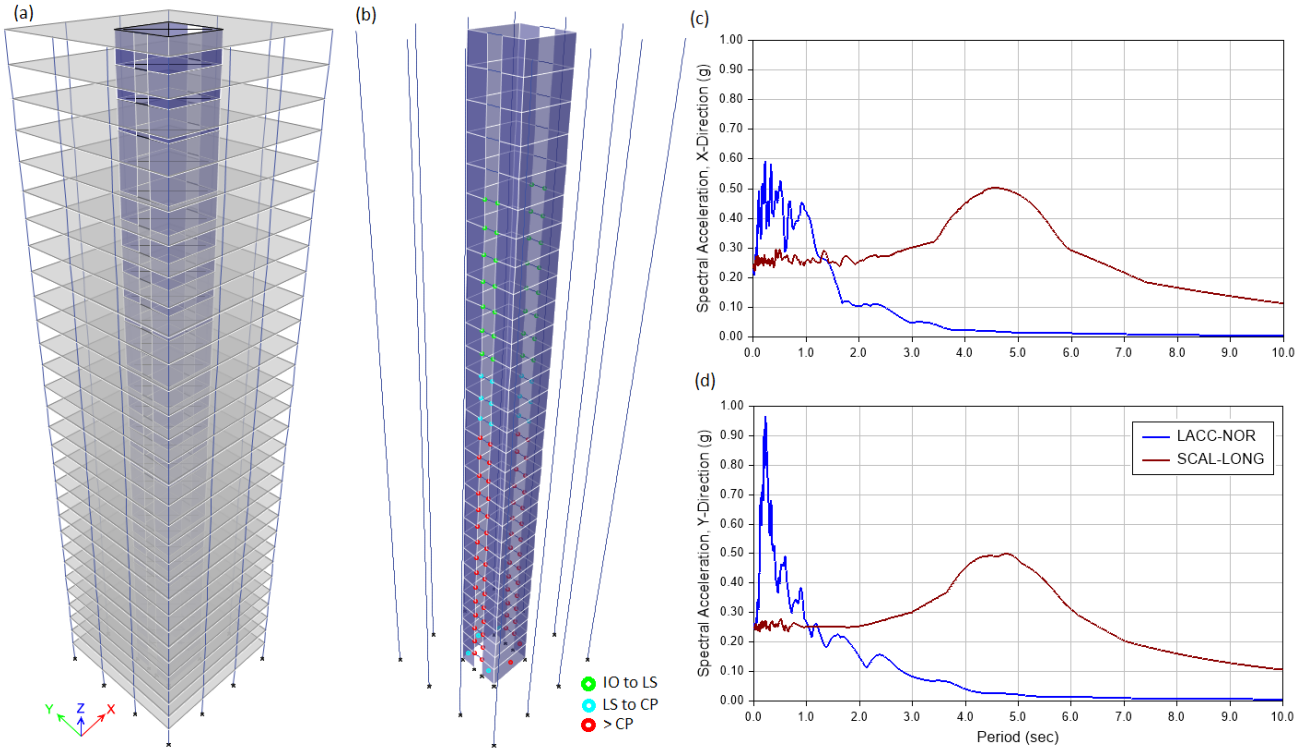

Fig. 6 – (a) 30-story core wall building modeled in ETABS; (b) Deformed shape at time t = 17.5 sec for ground motion excitation "SCAL-LONG" with modal damping, floors are not shown for clarity; (c) X- and (d) Y-direction spectral accelerations for the ground motion excitations LACC-NOR (unscaled) and SCAL-LONG.

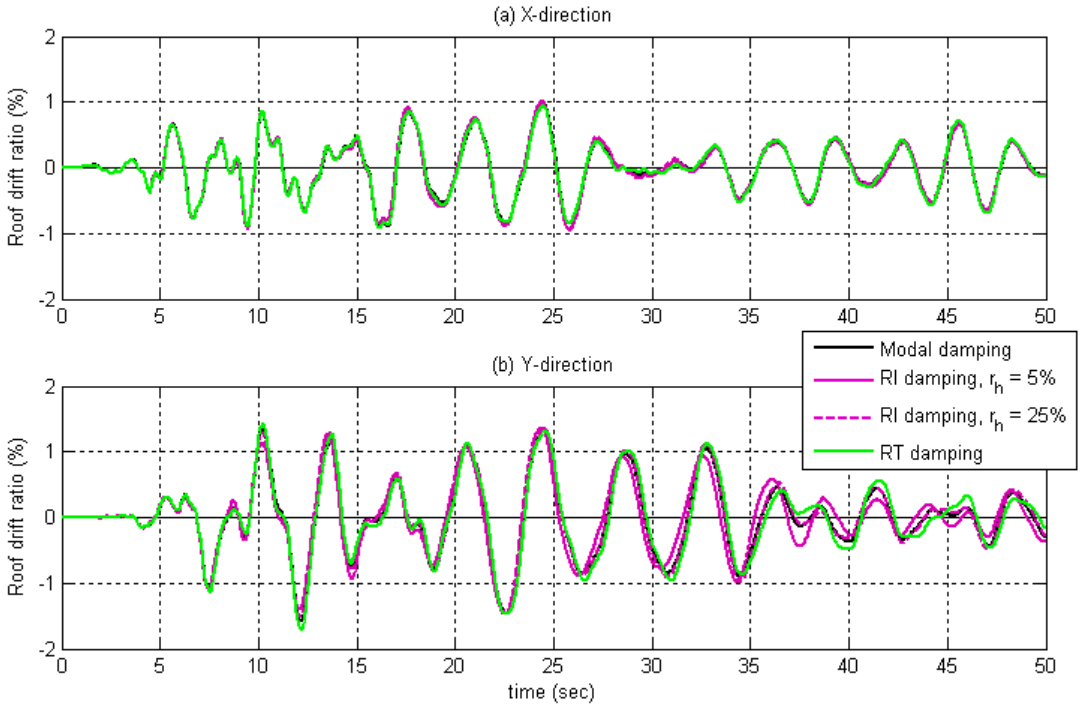

Fig. 7 – Roof drift response time history of 30-story building model for base excitation LACC-NOR in the (a) X- and (b) Y-directions with RI, RT, and modal damping.

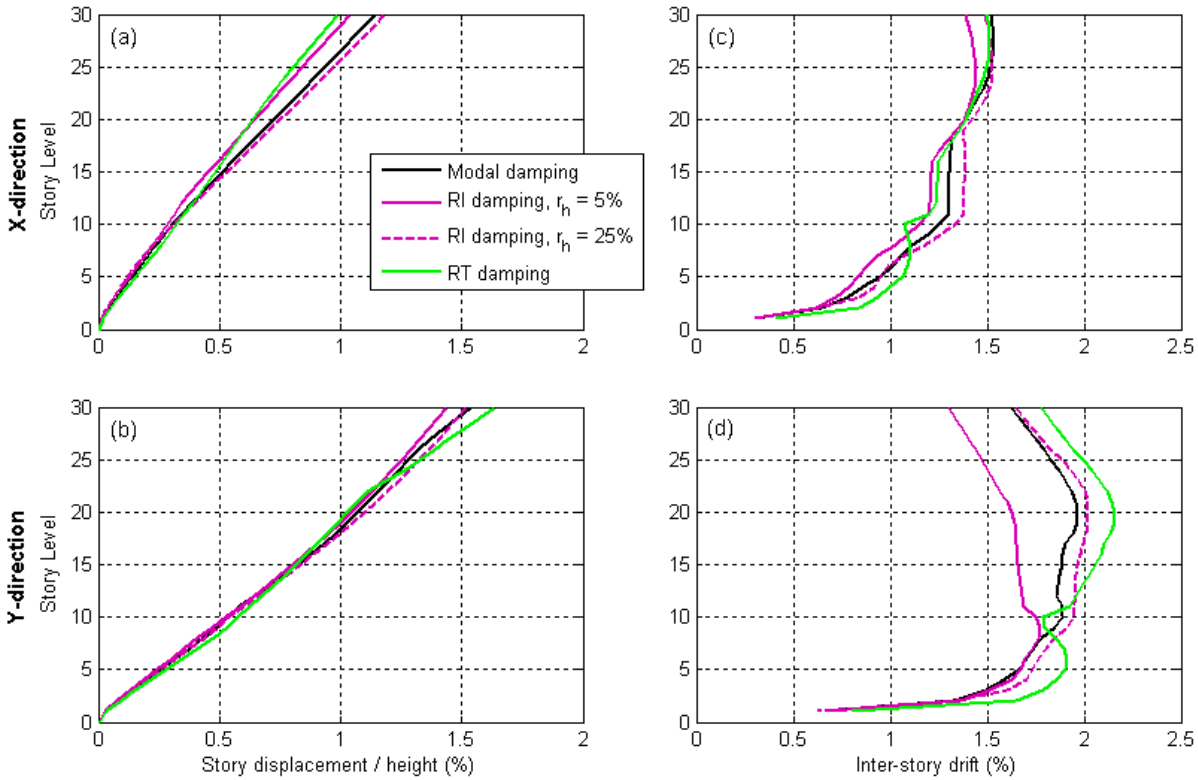

Fig. 8 – Peak response values of (a-b) floor displacements normalized by the total building height and (c-d) inter-story drift ratio of 30-story building model for base excitation LACC-NOR with RI, RT, and modal damping.

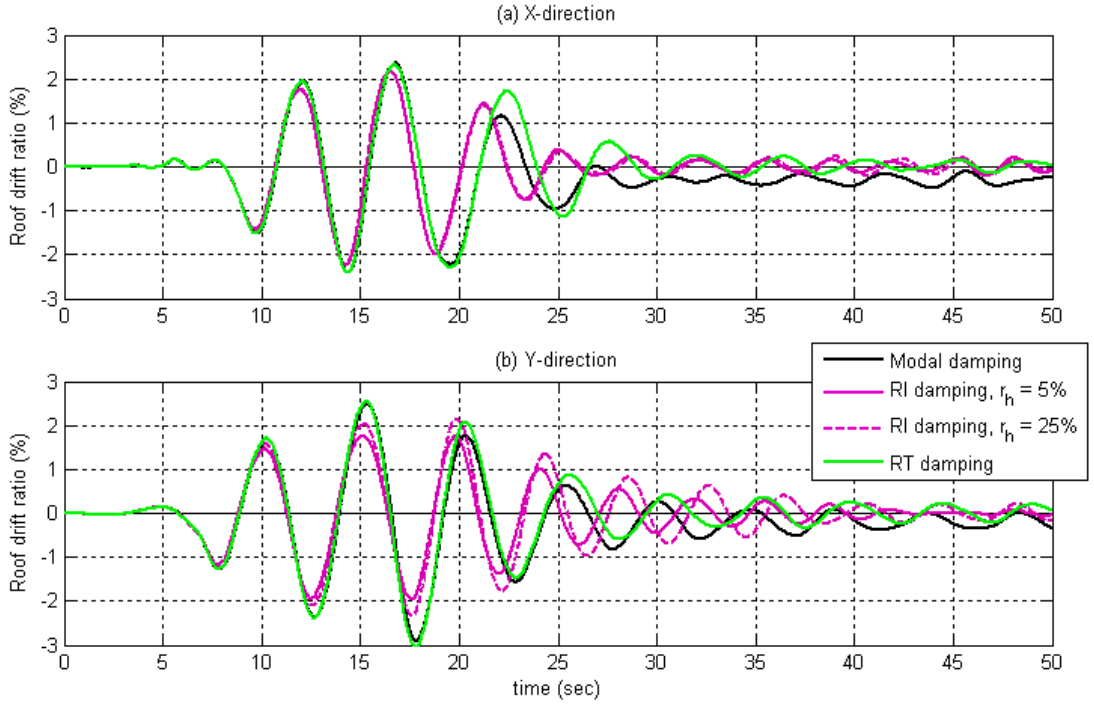

Fig. 9 – Roof drift response time history of 30-story building model for base excitation SCAL-LONG in the (a) X- and (b) Y-directions with RI, RT, and Modal damping.

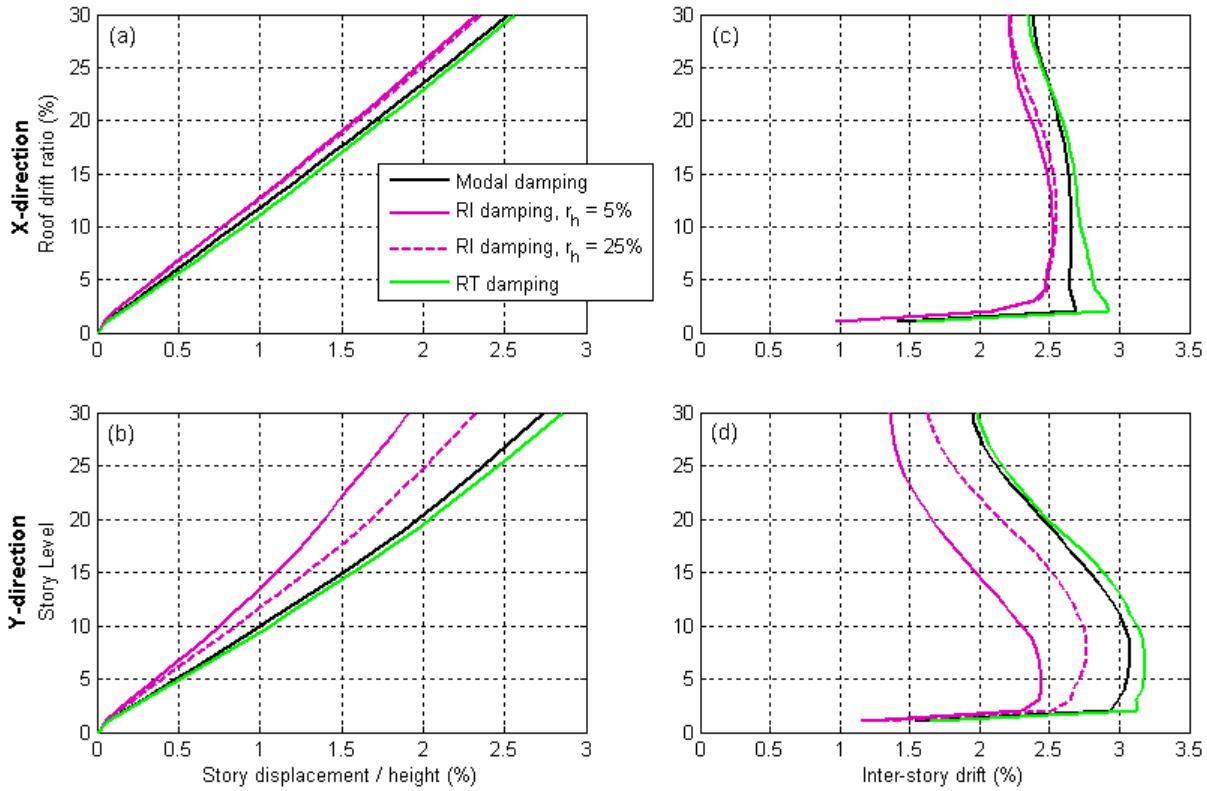

Fig. 10 – Peak response values of (a-b) floor displacements normalized by the total building height and (c-d) inter-story drift ratio of 30-story building model for base excitation SCAL-LONG with RI, RT, and modal damping.

Figures 7 and 8 shows the roof drift response time history and peak values of floor displacement and inter-story drift ratio in the X- and Y- directions for ground motion excitation LACC-NOR. The three considered damping methods do not result in large differences for the computed roof drift response: the RI with r_h = 5%, RI with r_h = 25%, and modal damping peak roof drift were 1.05, 1.2, and 1.16 times that of RT damping, respectively, in the X-direction and 0.88, 0.93, and 0.94 times that of RT damping, respectively, in the Y-direction. The inter-story drift response showed greater differences; the results of RI with r_h = 25% and modal damping had good agreement. As an average over the height for the X- and Y-directions, inter-story drift ratios from modal damping had a 5.8% and 9% difference, respectively, from that of RT damping. Comparatively, inter-story drift ratios from RI damping with r_h = 25% had a 6.6% and 8% difference, respectively, from that of RT damping.

Figures 9 and 10 shows the roof drift response time history and peak values of floor displacement and inter-story drift ratio in the X- and Y- directions for ground motion excitation SCAL-LONG. The damage from this ground motion excitation is extensive; the hinge states and deformed shape (deformation scale factor = 1) of the building at time t = 17.5 sec are shown in Figure 6(b). The coupling beams over the bottom half of the building have exceeded the collapse prevention (CP) state and have begun to lose moment strength capacity. The damage to the core walls is concentrated at the bottom two stories of the building, forming a flexible plastic hinge at the base of the building. For this ground motion excitation, the results with modal damping agree well with that of RT damping while RI damping, especially with r_h = 5%, computes significantly smaller displacement and drift response. The RI with r_h = 5%, RI with r_h = 25%, and modal damping peak roof drift were 0.91, 0.92, and 0.98 times that of RT damping, respectively, in the X-direction and 0.67, 0.81, and 0.96 times that of RT damping, respectively, in the Y-direction. As an average over the height, inter-story drift ratios from modal damping had a 2.6% and 2.9% difference from that of RT damping in the X- and Y-directions, respectively. Comparatively, inter-story drift ratio from RI damping with r_h = 5% and 25% exceeded 10% and 8% difference, respectively, from that of RT damping in either direction. This behavior is consistent with the results of the building with lumped plasticity studied by McKenna and Chopra [3]; in that study, the modal damping was done with direct-integration time history analysis. In addition, the effect of hinge discretization is apparent on the results in the Y-direction, the direction of loading corresponding to deformation of the coupling beams.

Table 2 lists the computational time for the analysis with each of the three damping methods and two ground motions excitations. While analysis with RT damping is 3-5 times slower than RI damping, modal damping with the FNA method is considerably faster than both: 8 and 3.4 times faster than RI damping for LACC-NOR and SCAL-LONG, respectively.

Table 2 – Analysis computational time (sec) for the 30-story building model subjects to ground motion excitation LACC-NOR and SCAL-LONG (using a 3.49 GHz Intel Xeon CPU and 24 GB of RAM).

Damping Model	Computational time (sec)	
	LACC-NOR	SCAL-LONG
RI, r_h = 5%	4113	1668
RI, r_h = 25%	3750	1674
RT	18418	6106
Modal	482	489

5. Conclusion

Compared to the Rayleigh damping methods for nonlinear time history analysis, modal damping has the advantage of being readily understood and controlled because the modal damping ratios can be specified independently for each mode. While modal damping can be used in direct-integration analysis, this paper considered its use in nonlinear modal time-history analysis (FNA) methods.

Similar to tangent stiffness proportional Rayleigh (RT) damping, modal damping is shown to be insensitive to hinge discretization and does not produce spurious damping forces at nodes with little or no mass, both of which are major concerns for initial stiffness proportional Rayleigh (RI) damping. While discretization effects can be

reduced by modeling techniques, they can be still be inherent in the structural configuration such as due to localized damage or hinging at the first story of a tall building.

One limitation to modal damping is that the damping matrix is constructed based on the initial modal properties of the structure so that inelastic modes may be more damped than expected when stiffness reduction occurs on a global level. However, in the case study of a 30-story building model subjected to two different bi-axial ground motions, modal damping with FNA was shown to produce displacement and inter-story drift results similar to RT damping while RI damping significantly underestimated the displacements and drifts for the larger earthquake excitation. Analysis using FNA with modal damping was shown to be more than 10 times faster than using direct-integration with RT damping, and was more than 3 times faster than RI damping.

6. Acknowledgements

The authors wish to acknowledge the generous support of Computers and Structures, Inc. in the preparation of this paper, along with critical input from Ashraf Habibullah.

7. References

[1] Bernal D (1994): Viscous damping in inelastic structural response. *Journal of Structural Engineering*, **120** (4), 1240-1254.

[2] Charney F (2008): Unintended consequences of modeling damping in structures. *Journal of Structural Engineering*, **134** (4), 581-592.

[3] Chopra AK, McKenna F (2015): Modeling viscous damping in nonlinear response history analysis of buildings for earthquake excitation. *Earthquake Engineering & Structural Dynamics*, **45** (2), 193-211.

[4] *CSI Analysis Reference Manual for SAP2000, ETABS, SAFE, and CSiBridge*, July 2015. Walnut Creek, CA: Computers & Structures, Inc.

[5] Erduran E (2012): Evaluation of Rayleigh damping and its influence on engineering demand parameters. *Earthquake Engineering & Structural Dynamics*, **41** (14), 1905-1919.

[6] *ETABS* [computer program]. Version 15.2.2. Walnut Creek, CA: Computers & Structures, Inc.

[7] Hall JF (2006): Problems encountered for the use (or misuse) of Rayleigh damping. *Earthquake Engineering & Structural Dynamics*, **35** (5), 525-545.

[8] Hardyniec A, Charney F (2015): An investigation into the effects of damping and nonlinear geometry models in earthquake engineering analysis. *Earthquake Engineering & Structural Dynamics*, **44** (15), 2695-2715.

[9] Ibrahimbegovic A, Wilson EL (1989): Simple numerical algorithms for the mode superposition analysis of linear structural systems with non-proportional damping. *Computers and Structures*, **33** (2), 523-531.

[10] Jehel P, Leger P, Ibrahimbegovic A (2014): Initial versus tangent stiffness-based Rayleigh damping in inelastic time history seismic analyses. *Earthquake Engineering & Structural Dynamics*, **43** (3), 467-484.

[11] *OpenSEES* [computer program]. Version 2.5.0. Berkeley, CA: University of California, Berkeley.

[12] Pant DR, Wijeyewickrema AC, El Gawady MA (2013): Appropriate viscous damping for nonlinear time-history analysis of base-isolated reinforced concrete buildings. *Earthquake Engineering & Structural Dynamics*, **42** (15), 2321-2339.

[13] *Perform-3D* [computer program]. Version 5.0.1. Walnut Creek, CA: Computers & Structures, Inc.

[14] Petrini L, Maggi C, Priestley MJN, Calvi GM (2008): Experimental verification of viscous damping modeling for inelastic time history analyzes. *Journal of Earthquake Engineering*, **12** (S1), 125-145.

[15] Wilson EL (2010): *Static and Dynamic Analysis of Structures: A Physical Approach with Emphasis on Earthquake Engineering*. Computers & Structures, Inc, 4th edition.

[16] Wilson EL, Penzien J (1972): Evaluation of orthogonal damping matrices. *International Journal for Numerical Methods in Engineering*, **4** (1), 5-10.

[17] Zareian F, Medina RA (2010): A practical method for proper modeling of structural damping in inelastic plane structural systems. *Computers and Structures*, **88** (1), 45-53.